


Article

The Effect of Heat Treatment on Properties of Ni–P Coatings Deposited on a AZ91 Magnesium Alloy

Martin Buchtík , Michaela Krystýnová, Jiří Másilko and Jaromír Wasserbauer

Materials Research Centre, Faculty of Chemistry, Brno University of Technology, Purkyňova 464/118, 61200 Brno, Czech Republic

* Correspondence: xcbuchtik@fch.vut.cz; Tel.: +420-736-445-019

Received: 10 June 2019; Accepted: 19 July 2019; Published: 23 July 2019



Abstract: The present study reports the effect of phosphorus content in deposited electroless nickel (Ni–P) coatings, the heat treatment on the microhardness and its microstructural characteristics, and the influence of the temperature on the microstructure of the Mg alloy substrate during the heat treatment. The deposition of Ni–P coatings was carried out in the electroless nickel bath, and the resulting P content ranged from 5.2 to 10.8 wt.%. Prepared samples were heat-treated in the muffle furnace at 400 °C for 1 h after the coating deposition. The cooling of the samples to room temperature was proceeded in the air. For as-deposited and heat-treated samples, it was determined that with the increasing P content, the microhardness was decreasing. This may be caused by the changes in the structure of the Ni–P coating. The X-ray diffraction patterns of the as-deposited Ni–P coatings showed that the microstructure changed their nature from crystalline to amorphous with the increasing P content. The heat treatment of prepared samples led to the significant increase of microhardness of Ni–P coatings. All the heat-treated samples showed the crystalline character, regardless of the P content and the presence of hard Ni₃P phase, which can have a positive effect on the increase of microhardness. The metallographic analysis showed changes of substrate microstructure after the heat treatment. The prepared coatings were uniform and with no visible defects.

Keywords: Ni–P coatings; Ni₃P phase; Mg alloys; AZ91; heat treatment; microhardness; crystallite size

1. Introduction

Magnesium alloys are the lightest structural metallic materials [1,2]. Due to their exceptional properties, such as a low density, stiffness, specific strength, good castability, and machinability, they are desirable in various industries [3–5]. One of the biggest limits for the widespread use of magnesium alloys is their poor corrosion, wear resistance, and low hardness [1,5–7]. These problems are often resolved by means of surface coatings. Electroless nickel (Ni–P) deposition seems to be an appropriate variant to protect magnesium alloy substrates [8]. Electroless Ni–P coatings are mainly used due to their excellent corrosion resistance, high hardness, and wear resistance. However, properties of Ni–P coatings are strongly dependent on their chemical composition, i.e., the phosphorus (P) content in the coating [9]. In terms of the chemical composition, electroless Ni–P coatings can be divided into three groups: Low phosphorus (1–5 wt.% of P), medium phosphorus (6–9 wt.% of P), and high phosphorus (10–13 wt.% of P) [9–11]. Low phosphorus Ni–P coatings are predominantly crystalline and less corrosion resistant compared to the medium and high P coatings. They are characteristic with a high hardness and good mechanical and tribological properties. The crystalline character of the low phosphorus coatings indicates that the number of phosphorus atoms in interstitial positions is not sufficient for the distortion of the nickel lattice [11,12].

High phosphorus Ni–P coatings are known for excellent corrosion resistance due to their amorphous microstructure [11–13].

Duncan [11] stated that Ni–P coating is in non-equilibrium state after deposition. Ni–P coating is formed by a crystalline solid solution of P in Ni, called the β phase (low phosphorus), the total amorphous γ phase, which exists between 11–15 wt.% P (high phosphorus), or the mixture of $\beta + \gamma$ phase (medium phosphorus). These metastable phases are characterized by decomposition reactions during the heat treatment to form the equilibrium α phase (solid solution of P in Ni) and Ni_3P phase. Crystalline nickel (the α phase) and the Ni_3P phase are only stable products after the heat treatment. These stable phases begin to form from 300 °C. The optimal temperature range for the heat treatment of the Ni–P coatings is within the temperature range of 300 to 400 °C. Riedel [10] stated that it is advisable to perform heat treatment at 400 °C for 1 h to achieve the maximum hardness of Ni–P coatings. The increase in precipitate size and coating grain coarsening was observed at applied temperatures higher than 400 °C and longer treating times during the heat treatment process, regardless of the P content [14,15].

A suitable heat treatment process can result in an increase in the coating hardness, up to 1300 HV. This is because of the recrystallization of a non-equilibrium β phase (low phosphorus), an amorphous γ phase (high phosphorus), or their mixture (medium phosphorus) into the equilibrium crystalline α phase, with a simultaneous precipitation of the hard intermediate Ni_3P phase [10,14].

Kumar [16] reported that the crystallite size of Ni changes with the increasing heat treatment temperature. From the room temperature to 100 °C, there was only a negligible change in the Ni crystallite size. Between 100 and 300 °C, the increase in crystallite size of Ni was evident due to the arrangement of Ni atoms in the lattice. However, no formation of any intermediate precipitate particles was detected. Authors also listed that the disappearance of the amorphous phase was observed at 330 °C, what indicates the complete crystallization of the microstructure. At a temperature above 300 °C, a significant increase in crystallite size was observed, probably due to the formation of Ni_3P phase particles.

Most of the published studies are focused on the influence of heat treatment and P content in Ni–P coatings deposited on the steels. However, the heat treatment of Ni–P coatings to achieve the maximum hardness is performed in the temperature of 400 °C for 1 h. This temperature does not influence the microstructure of steels but may have significant effect on magnesium alloys. Therefore, this study deals with the effects of the heat treatment of Ni–P coatings with the various P content deposited on a AZ91 magnesium alloy. The microstructure of a AZ91 alloy and the characterization of Ni–P coatings, such as microhardness, phase composition, and crystallite size, were evaluated before and after the heat treatment.

2. Materials and Methods

Samples of a cast AZ91 magnesium alloy with dimensions of $30 \times 30 \times 7 \text{ mm}^3$ were chosen as substrates for the electroless deposition of Ni–P coatings. The elemental composition of the AZ91 alloy, analyzed using the glow-discharge optical emission spectroscopy (GDOES) Spectrumat GDS 750 (Spectrums Analytik GmbH, Hof, Germany), is listed in Table 1. To obtain an appropriate surface, the samples of the Mg alloy were ground using no. 1200 SiC paper before the pre-treatment process. During the pre-treatment process, ground samples were degreased in an alkali bath and then pickled in an acid-pickling bath to activate the surface. After each step of the pre-treatment, samples were rinsed in distilled water and isopropyl alcohol and then dried in hot air. The deposition of Ni–P coatings was carried out in the electroless nickel bath with different $\text{Ni}^{2+}/\text{H}_2\text{PO}_2^-$ ratios. Individual ratios of $\text{Ni}^{2+}/\text{H}_2\text{PO}_2^-$ were set at 0.1, 0.2, 0.3, 0.45, and 0.75. The chemical composition was characterized using a Zeiss EVO LS-10 (Carl Zeiss Ltd., Cambridge, UK) scanning electron microscope (SEM) with energy-dispersive spectroscopy (EDS) Oxford Instruments Xmax 80 mm^2 detector (Oxford Instruments plc, Abingdon, UK) and the AZtec software (version 2.4).

Table 1. Elemental composition of the AZ91 Mg alloy, glow-discharge optical emission spectroscopy (GDOES).

Element	Al	Zn	Cu	Mn	Si	Fe	Ni	Zr	Mg
Content [wt.%]	8.80	0.81	0.00	0.32	0.01	0.004	0.00	0.01	Bal.

Prepared samples were heat-treated in the muffle furnace LAC LM07 (LAC, s.r.o., Židlochovice, Czech Republic) at 400 °C for 1 h after the coating deposition. The cooling of the samples to room temperature was proceeded in the air.

The microstructure of the Ni–P coatings and AZ91 magnesium alloy was characterized using an Axio Observer Z1m (ZEISS) light microscope and a Zeiss EVO LS-10 scanning electron microscope.

The microhardness of the deposited Ni–P coatings was measured using a LECO AMH55 microhardness tester (Saint Joseph, MO, USA). The microhardness was performed and evaluated according to the ASTM E384 standard. The microhardness was measured from the perpendicular cut. The samples were ground and polished using a Tegramin-25 (Struers) automatic grinder with a special holder for preparation of planar specimens. The final step was polishing, using diamond paste with 0.25 µm particle size. Iso-propanol was used as a lubricant. The Vickers method was used with the applied load of 25 g for 10 s. The microhardness value was determined from 10 values.

For the determination and characterization of the Ni–P coatings phase composition, the coatings were mechanically separated from the substrate, milled, and analyzed in the powder form using the Scherrer method. The analysis was performed on an Empyrean (Panalytical) X-Ray diffraction spectrometer with Cu-anode ($\lambda K\alpha_1 = 0.15406$ nm, $\lambda K\alpha_2 = 0.15444$ nm) at room temperature. The scan step size was set up at 0.013°. The obtained data were processed using High Score Plus software. The crystallite size of Ni and Ni₃P was calculated from the full width half maximum (FWHM) according to the Scherrer equation [17] (Equation (1)):

$$\tau = \frac{K \cdot \lambda}{\beta_{1/2} \cdot \cos \theta} \quad (1)$$

where τ is the crystallite size, λ is the X-ray wavelength, $\beta_{1/2}$ is the peak extension at half of the maximum intensity (FWHM), θ is the diffraction Bragg's angle, and K is the particles shape factor (Scherrer constant) depending on the shape of the crystallites. K , ranging from 0.62 to 2.08, is usually close to 1. For perfectly rounded crystals, K is equal to 0.89.

3. Results and Discussion

3.1. Microstructure and Chemical Composition

Table 2 shows the results of the chemical composition of the as-deposited and heat-treated Ni–P coatings, deposited on the AZ91 alloy with different Ni²⁺/H₂PO₂[−] ratios in the electroless nickel bath. The average phosphorus content in as-deposited and heat-treated coatings was similar for the same Ni²⁺/H₂PO₂[−] ratios, therefore there is only one value for each Ni²⁺/H₂PO₂[−] ratio. The average P content ranges from approximately 5 wt.% to 11 wt.% of P, both for as-deposited and heat-treated coatings.

Table 2. The phosphorus content of electroless nickel (Ni–P) as-deposited and heat-treated coatings in dependence on the Ni²⁺/H₂PO₂[−] ratios, energy-dispersive spectroscopy (EDS).

Ni ²⁺ /H ₂ PO ₂ [−] Ratio	P Content [wt.%]
0.75	5.2 ± 0.2
0.45	5.5 ± 0.1
0.3	7.4 ± 0.1
0.2	10.1 ± 0.2
0.1	10.8 ± 0.1

Figure 1 shows the microstructure of as-deposited and heat-treated Ni–P. The microstructures of as-deposited and heat-treated Ni–P coatings were similar, regardless of the chemical composition. The average thickness of all coatings was approximately 30 μm . The coating was uniform without structural defects and there was no undesirable interlayer between the magnesium alloy substrate and Ni–P coating. The heat treatment did not affect the thickness or overall chemical composition of the deposited Ni–P coatings.

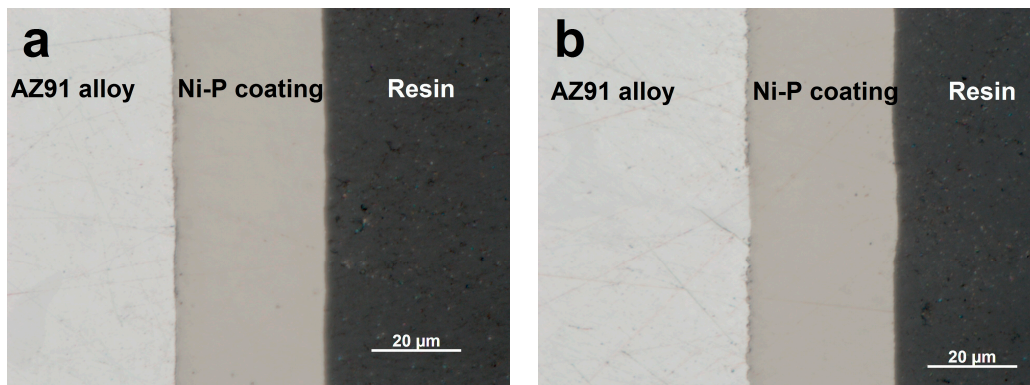


Figure 1. Microstructure of Ni–P coatings with 7.4 wt.% P (a) as-deposited; (b) heat-treated.

As shown in Figure 2a, the microstructure of the cast AZ91 magnesium alloy consists of (1) α solid solution of Al in Mg, (2) discontinuous precipitates of intermetallic $\text{Mg}_{17}\text{Al}_{12}$ - β_{D} phase, and (3) eutectic $\alpha + \beta$ [1,2].

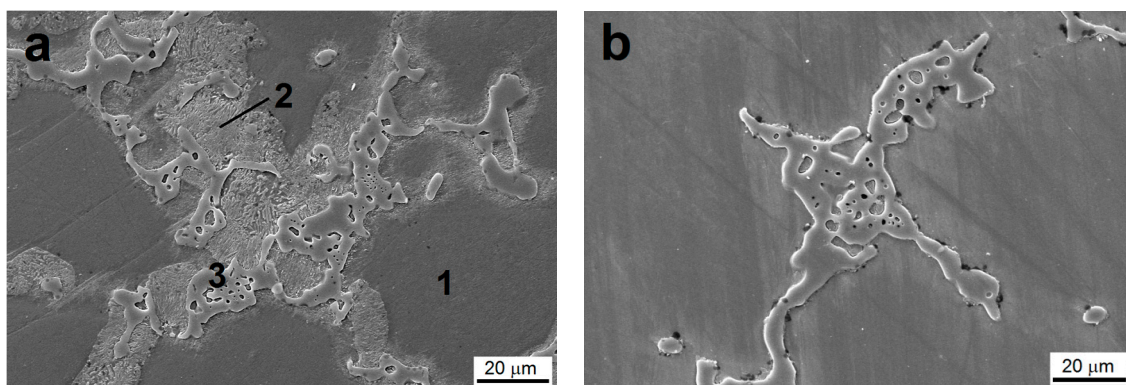


Figure 2. Microstructure of the AZ91 Mg alloy (a) as-cast, (b) heat-treated at 400 °C for 1 h.

In the case of heat-treated samples, the microstructure of the AZ91 alloy was changed. As seen in Figure 2b, the presence of the discontinuous precipitate of the $\text{Mg}_{17}\text{Al}_{12}$ phase was not observed. This finding can be explained by the fact that the discontinuous precipitate was dissolved in α solid solution of Al in Mg during the heat treatment at 400 °C for 1 h. Due to the fast cooling in the air after being removed from the furnace, discontinuous precipitates of the $\text{Mg}_{17}\text{Al}_{12}$ - β_{D} phase were not present [2]. However, the $\text{Mg}_{17}\text{Al}_{12}$ - β phase and eutectic $\alpha + \beta$ was still observed in the microstructure.

Because of the dissolution of the discontinuous precipitates of the $\text{Mg}_{17}\text{Al}_{12}$ - β_{D} phase at 400 °C, the content of Al in the α solid solution increased, which may lead to improvement of some mechanical properties due to the solid solution strengthening.

3.2. Microhardness of Ni–P Coatings

As stated in the literature [10,18], low-phosphorus Ni–P coatings are crystalline, medium-phosphorus coatings are microcrystalline, and high-phosphorus Ni–P coatings are amorphous. The microstructure of deposited Ni–P coatings strictly affects their properties [12,13]. In general, the microhardness decreases with the increasing P content.

From the results of microhardness, the measurement can be stated that the highest microhardness value was observed in the case of the Ni–P coating with the lowest P. With the increasing P content, the microhardness decreased in the case of both the as-deposited and in the heat-treated coatings (Figure 3), which is in correlation with the literature [12,13,19]. Ashtiani et al. [19] reported that in the case of the Ni–P coatings heat-treated at 400 °C, the microhardness decreased with the increasing P content, which is in agreement with presented data. Deposited Ni–P coating with 9.35 wt.% of P reached the microhardness of 970 HV 50 gf. Meanwhile, the coatings with 10.31 and 11.45 wt.% of P reached the microhardness of 856 HV 50 gf and 788 HV 50 gf, respectively.

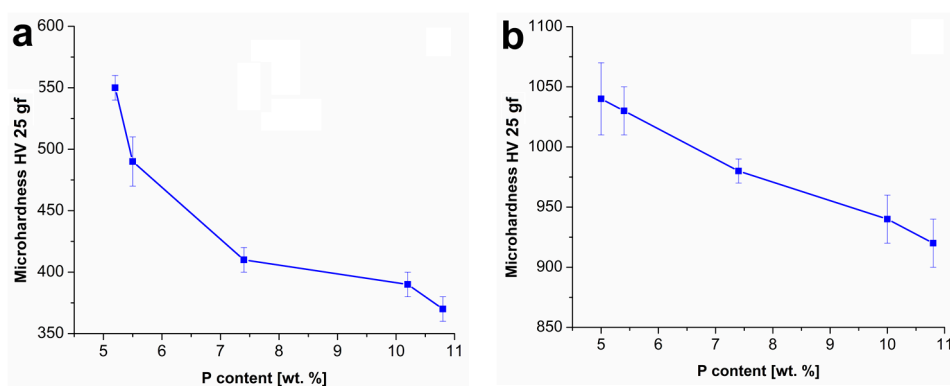


Figure 3. Microhardness dependence on the phosphorus content of Ni–P coatings, (a) as-deposited, (b) heat-treated.

Figure 3b shows that the heat-treated Ni–P coatings had higher value of microhardness when compared to the as-deposited coatings with the same P content. During the heat treatment, all the coatings (depending on the P content) became more crystalline due to the rearrangement of the structure and the transformation of the non-equilibrium solid solution P in the Ni- β phase (low phosphorus), total amorphous γ phase (high phosphorus), or their mixture (medium phosphorus) to equilibrium crystalline solid solution P in Ni- α phase. Simultaneously, heat treating lead to the formation of the hard body centered tetragonal Ni_3P phase. The presence of Ni_3P results in an overall increase of the microhardness of the coatings [9,10]. The presence of the Ni_3P phase in the heat-treated coatings was confirmed by XRD analysis.

3.3. Phase Analysis of Ni–P Coatings

The XRD patterns corresponding to the individual measurements representing Ni–P coatings are provided in Figure 4. As seen in the Figure 4a, the peak corresponding to the fcc nickel crystal lattice (1 1 1) can be observed near the diffraction angle $2\theta \approx 45^\circ$. A broad peak corresponding to the Ni diffraction was observed in the case of high-phosphorus coatings, and with the decreasing P content, the peak of Ni became sharper. This effect indicates a more ordered internal microstructure [18]. The highest intensity of Ni diffraction was measured for the Ni–P coating with 5.5 ± 0.1 wt.% of P. Meanwhile, the lowest intensity and the broadest peak was observed in the case of the Ni–P coating with 10.8 ± 0.1 wt.% of P.

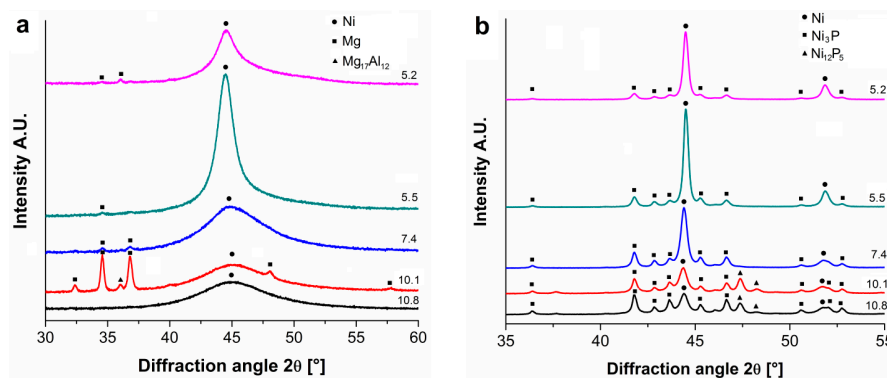


Figure 4. XRD patterns of (a) as-deposited and (b) heat-treated Ni–P coatings with different phosphorus content.

Except for the diffraction of Ni, there were clear diffractions between 30° – 40° and around the angle $2\theta \approx 48^{\circ}$. Gu [20] listed that these XRD peaks correspond to the primary α -Mg phase and the $\text{Mg}_{17}\text{Al}_{12}$ phase. The α -Mg phase was also detected in the work of Hu [21].

The presence of the phase particles can be explained by the fact that there was a joint separation of the Mg alloy together with the Ni–P coating during the mechanical separation. However, the presence of these phases in the tested powder did not affect the microstructural changes observed in deposited Ni–P coatings.

Figure 4b shows the patterns of heat-treated Ni–P coatings with different P content. The diffraction of Ni (1 1 1) can be seen near the diffraction angle $2\theta \approx 44.4^{\circ}$. Another diffraction of Ni (2 0 0) can be seen at $2\theta \approx 51.8^{\circ}$. For both of the Ni diffractions, it can be observed that their intensity increases and peaks become more sharp with the decreasing P content (except the P content 5.2 ± 0.2 wt.%, which is slightly lower than the peak for the Ni–P coating with the P content 5.5 ± 0.1 wt.%).

Figure 4b shows that the presence of the Ni_3P stable phase was obvious for all the coatings and the intensity of the Ni_3P phase increased with the increasing P content. From patterns shown in Figure 4b, it is evident that in the case of low-phosphorus Ni–P coatings, the Ni phase crystallizes more (the peak of Ni is sharper and with higher intensity) when compared to the high-phosphorus Ni–P coatings. On the other hand, the Ni_3P phase precipitated and grew more in the case of the high-phosphorus Ni–P coating. The presence of the Ni_{12}P_5 metastable phase was observed in the case of high-phosphorus Ni–P coatings (10.2 and 10.8 wt.% of P) around the diffraction angle $2\theta \approx 47^{\circ}$ to 48° . According to the literature [22,23], the Ni_{12}P_5 metastable phase should completely disappear around the temperature of 350°C . However, Keong [24] showed that the Ni_{12}P_5 phase may still be present at 400°C . The presence of this phase could be caused by the incomplete transformation from the originally amorphous matrix to the mixture of crystalline Ni and the Ni_3P stable phase.

3.4. Crystallite Size

Figure 5 shows the effect of the phosphorus content on the Ni crystallite size in as-deposited coatings and heat-treated coatings. Only one diffraction plane Ni (1 1 1) was observed (see Figure 4a) and two diffraction planes (1 1 1) and (2 0 0) of Ni were observed (Figure 4b) in the case of as-deposited and heat-treated coatings by XRD, respectively. Figure 5 shows that with the increasing P content, the crystallite size of nickel decreases, both in the case of the as-deposited and heat-treated coatings. This fact can be explained due to the increasing lattice disorder (a greater proportion of the amorphous phase) with the increasing P content in the Ni–P matrix [12,24].

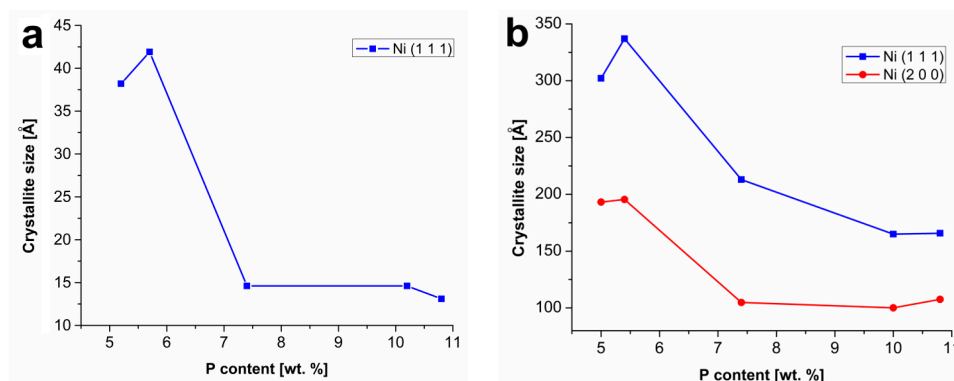


Figure 5. The effect of Ni crystallite size on the P content in (a) as-deposited Ni–P coatings and (b) heat-treated Ni–P coatings.

As can be seen in Figure 5a, the crystallites of Ni in low-phosphorus as-deposited Ni–P coatings reached approximately 40 Å, whereas the crystallites of Ni in the Ni–P coating with 10.8 wt.% of P reached the size of 13.1 Å. After the heat treatment, the crystallite size of Ni substantially increased to more than 300 Å in the case of low-phosphorus coatings in the plane (1 1 1). A similar trend was observed for the diffraction plane (2 0 0).

On the other hand, in the case of the heat-treated Ni–P coatings, the Ni_3P crystallite size increased with the increasing P content, as seen in Figure 6. The Ni_3P crystallite size dependence on the P content was studied for diffractions with the highest intensity. The most distinctive diffraction angles were $2\theta \approx 41.7^\circ, 42.8^\circ, 43.6^\circ, 45.3^\circ, 46.6^\circ$, and 52.7° , which corresponds to the diffraction planes (3 2 1), (3 3 0), (1 1 2), (4 2 0), (1 4 1), and (3 1 2), respectively. Increasing crystallite size of Ni_3P is related to increasing P content. With a higher P content, a Ni_3P phase fraction is formed and combined to form coarser particles. Meanwhile, in the case of low phosphorus coatings, the formed Ni_3P phase is in the form of fine-grained precipitates distributed in the Ni–P matrix.

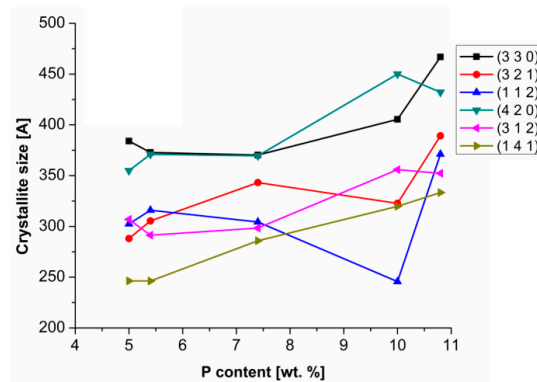


Figure 6. The effect of Ni_3P crystallite size on the P content in heat-treated Ni–P coatings.

Based on the literature [10,14], it is evident that the chemical composition and the size of the Ni_3P phase can affect the resulting microstructure and hardness of the Ni–P coatings.

Higgs [18] states that the heat-treated coatings showed fine-grained intermetallic precipitates of Ni_3P in the Ni–P matrix. The author also pointed out that the size of Ni_3P precipitates in the Ni–P matrix depended on the temperature. According to our study, the size of Ni_3P precipitates is also related to the P content (Figure 6).

Finer precipitates of Ni_3P may be responsible for the increased hardness or the improvement of other mechanical properties [14,25]. With reference to measured results of microhardness of the Ni–P coatings (Figure 3) and their microstructural characteristics (Figures 5 and 6), it is evident that the microhardness depends not only on the P content, but also on the size and distribution of Ni_3P .

precipitates in the case of heat-treated coatings. Therefore, the heat treatment leads to a significant increase of microhardness of the Ni–P coatings.

However, the heat treatment also affects the substrate. The temperature of 400 °C influences the structure of Mg alloys more than in the case of steels. The heat treatment of the AZ91 alloy led to the dissolution of the discontinuous precipitate $Mg_{17}Al_{12}$. The difference in the thermal expansion coefficient of AZ91 Mg alloy and the Ni–P coating may lead to tension at the interface. However, there was no observable impact (visible cracks or delamination) at the Mg substrate/Ni–P coating interface.

4. Conclusions

The electroless Ni–P coatings with various P content were deposited on AZ91 Mg alloys and subsequently heat-treated at 400 °C for 1 h.

As-deposited Ni–P coatings showed the decrease in microhardness with increasing P content. Heat-treated Ni–P coatings showed a similar trend. However, the heat-treated coatings reached significantly higher microhardness values.

From the XRD analysis, it was determined that the microstructure of the as-deposited high-phosphorus coatings was amorphous, and with the decreasing P content they become more crystalline. Heat-treated Ni–P coatings were completely crystalline, and a presence of crystalline Ni and the intermediate Ni_3P phase in the coating was observed. It was observed that the Ni crystallite size in the coating decreased with the increasing P, both for as-deposited and heat-treated Ni–P coatings. On the other hand, the crystallite size of Ni_3P increased with increasing P content in the coating.

In terms of the precipitation hardening process, the heat-treated Ni–P coatings reached higher microhardness values than the as-deposited coatings. This is due to the presence of a large number of intermetallic precipitates of Ni_3P .

The influence of temperature during the heat treatment led to the dissolution of the discontinuous precipitate $Mg_{17}Al_{12}$. Despite the substrate microstructural changes and difference in thermal expansion coefficients, this did not lead to the delamination or visible cracking of the coating. The prepared coatings were uniform and with no visible defects.

Author Contributions: Conceptualization, M.B. and M.K.; methodology M.B., J.M. and J.W.; validation, M.B., M.K. and J.W.; formal analysis, M.B. and M.K.; investigation, M.B. and M.K.; resources, M.B. and J.W.; data curation, M.B. and J.M.; writing—original draft preparation, M.B.; writing—review and editing, M.B. and M.K. visualization, M.B. and M.K.; supervision, J.W.; project administration, J.W.; funding acquisition, J.W.

Funding: This work was supported by project Nr. LO1211, Materials Research Centre at FCH BUT- Sustainability and Development (National Program for Sustainability I, Ministry of Education, Youth and Sports).

Conflicts of Interest: The authors declare no conflict of interest.

References

1. Friedrich, H.; Mordike, B.L. *Magnesium Technology: Metallurgy, Design Data, Applications*; Springer: Berlin, Germany, 2006.
2. Czerwinski, F. *Magnesium Alloys: Design, Processing and Properties*; InTech: Rijeka, Croatia, 2011.
3. Buchtík, M.; Kosár, P.; Wasserbauer, J.; Tkacz, J.; Doležal, P. Characterization of electroless Ni–P coating prepared on a wrought ZE10 magnesium alloy. *Coatings* **2018**, *8*, 96. [[CrossRef](#)]
4. Ambat, R.; Zhou, W. Electroless nickel-plating on AZ91D magnesium alloy: Effect of substrate microstructure and plating parameters. *Surf. Coat. Technol.* **2004**, *179*, 124–134. [[CrossRef](#)]
5. Gray, J.E.; Luan, B. Protective coatings on magnesium and its alloys—A critical review. *J. Alloy. Compd.* **2006**, *336*, 88–113. [[CrossRef](#)]
6. Liu, Z.; Gao, W. The effect of substrate on the electroless nickel plating of Mg and Mg alloys. *Surf. Coat. Technol.* **2006**, *200*, 3553–3560. [[CrossRef](#)]
7. Tkacz, J.; Minda, J.; Fintová, S.; Wasserbauer, J. Comparison of electrochemical methods for the evaluation of cast AZ91 magnesium alloy. *Materials* **2016**, *9*, 925. [[CrossRef](#)] [[PubMed](#)]

8. Seifzadeh, D.; Mohsenabadi, H.K. Corrosion protection of AM60B magnesium alloy by application of electroless nickel coating via a new chrome-free pretreatment. *Bull. Mater. Sci.* **2017**, *40*, 407–415. [[CrossRef](#)]
9. Mallory, G.O.; Hajdu, J.B. *Electroless Coating: Fundamentals and Applications*; Noyes Publishing, William Andrew: Norwich, NY, USA, 2009.
10. Riedel, W. *Electroless Nickel Plating*; ASM International: Metals Park, OH, USA, 1991.
11. Duncan, R.N. The metallurgical structure of electroless nickel deposits: Effect on coating properties. *Plat. Surf. Finish.* **1996**, *8*, 65–69.
12. Agarwala, R.C.; Agarwala, V. Electroless alloy/composite coatings: A review. *Sadhana* **2003**, *3–4*, 475–493. [[CrossRef](#)]
13. Parkinson, R. *Properties and Applications of Electroless Nickel*; Nickel Development Institute: Toronto, ON, Canada, 1997.
14. Keong, K.G.; Sha, W.; Malinov, S. Hardness evolution of electroless nickel–phosphorus deposits with thermal processing. *Surf. Coat. Technol.* **2003**, *168*, 263–274. [[CrossRef](#)]
15. Sudagar, J.; Lian, J.; Sha, W. Electroless nickel, alloy, composite and nano coatings—A critical review. *J. Alloy. Compd.* **2013**, *571*, 183–204. [[CrossRef](#)]
16. Sampath Kumar, P.; Kesavan Nair, P. Studies on crystallization of electroless Ni–P deposits. *J. Mater. Process. Technol.* **1996**, *56*, 511–520. [[CrossRef](#)]
17. Niksefat, V.; Ghorbani, M. Mechanical and electrochemical properties of ultrasonic-assisted electroless deposition of Ni–B–TiO₂ composite coatings. *J. Alloy. Compd.* **2015**, *633*, 127–136. [[CrossRef](#)]
18. Higgs, C.E. The effect of heat treatment on the structure and hardness of an electrolessly deposited nickel–phosphorus alloy. *Electrodepos. Surf. Treat.* **1974**, *2*, 315–326. [[CrossRef](#)]
19. Ashtiani, A.; Faraji, A.S.; Amjad Iranaghi, S.; Faraji, A.H. The study of electroless Ni–P alloys with different complexing agents on Ck45 steel substrate. *Arab. J. Chem.* **2017**, *10*, 1541–1545. [[CrossRef](#)]
20. Gu, C.; Lian, J.; Li, G.; Niu, L.; Jiang, Z. Electroless Ni–P plating on AZ91D magnesium alloy from a sulfate solution. *J. Alloy. Compd.* **2005**, *391*, 104–109. [[CrossRef](#)]
21. Hu, B.; Sun, R.; Yu, G.; Liu, L.; Xie, Z.; He, X.; Zhang, X. Effect of bath pH and stabilizer on electroless nickel plating of magnesium alloys. *Surf. Coat. Technol.* **2013**, *228*, 84–91. [[CrossRef](#)]
22. Kundu, S.; Das, S.K.; Sahoo, P. Properties of electroless nickel at elevated temperature—A review. *Procedia Eng.* **2014**, *97*, 1698–1706. [[CrossRef](#)]
23. Mainier, F.B.; Fonseca, M.P.C.; Tavares, S.S.M.; Pardal, J.M. Quality of electroless Ni–P (Nickel–Phosphorus) coatings applied in oil production equipment with salinity. *J. Mater. Sci. Chem. Eng.* **2013**, *1*, 1–8. [[CrossRef](#)]
24. Keong, K.G.; Sha, W.; Malinov, S. Crystallisation kinetics and phase transformation behaviour of electroless nickel–Phosphorus deposits with high phosphorus content. *J. Alloy. Compd.* **2002**, *334*, 192–199. [[CrossRef](#)]
25. Guo, Z.; Keong, K.G.; Sha, W. Crystallisation and phase transformation behaviour of electroless nickel phosphorus platings during continuous heating. *J. Alloy. Compd.* **2003**, *358*, 112–119. [[CrossRef](#)]

